JMEPEG (2015) 24:3307–3314
DOI: 10.1007/s11665-015-1605-z

1059-9495/$19.00

Effects of Ultra Fast Cooling on Microstructure and Mechanical Properties of Pipeline Steels

Yong Tian, Qun Li, Zhao-dong Wang, and Guo-dong Wang

(Submitted February 26, 2015; in revised form May 2, 2015; published online July 16, 2015)

X70 (steel A) and X80 (steel B) pipeline steels were fabricated by ultra fast cooling (UFC). UFC processing improves not only ultimate tensile strength (UTS), yield strength (YS), yield ratio (YS/UTS), and total elongation of both steels, but also their Charpy absorbed energy (A_K) as well. The microstructures of both steels were all composed of quasi polygonal, acicular ferrite (AF), and granular bainite. MA islands (the mixtures of brittle martensite and residual austenite) are more finely dispersed in steel B, and the amount of AF in steel B is much more than that in steel A. The strength of steel B is higher than that of steel A. This is mainly attributed to the effect of the ferrite grain refinement which is resulted from UFC processing. The finely dispersed MA islands not only provide dispersion strengthening, but also reduce loss of impact properties to pipeline steels. UFC produces low-temperature transformation microstructures containing larger amounts of AFs. The presence of AF is a crucial factor in achieving desired mechanical properties for both steels. It is suggested that the toughness of the experimental steel increases with increasing the amount of AF.

Keywords acicular ferrite (AF), crack growth, pipeline steels, ultra fast cooling (UFC)

1. Introduction

To meet the increased demand of energy, large diameter, high-strength pipes are widely used for the purpose of improving energy transport efficiency (Ref 1-5). Strength and low-temperature toughness, weldability, resistance to hydrogen-induced cracking, and resistance to fatigue were the critical properties required in these types of steels (Ref 6). Therefore, the development of the novel pipeline steels, which are more environmentally friendly and more economical by low alloying, are essentially needed. Suitable combinations of microalloying additions contribute to an increase in strength directly through microstructural refinement, solid solution strengthening, and precipitation hardening, as well as indirectly, through enhanced hardenability and associated modification of the resulting microstructure (Ref 7). It has been demonstrated that by an appropriate control of processing parameters such as reheat temperature, rolling temperature, deformation per pass, cooling rate, etc., it is possible to obtain an optimum combination of strength and formability.

Recently, various types of low-carbon structural steel plates and pipeline steels were developed by the extensive use of thermomechanical controlled processing (TMCP), which has become the most powerful and effective manufacturing process to satisfy increased hardenability, improved strength, and superior low-temperature toughness (Ref 8, 9). TMCP continues to evolve to cope with the ever increasing demand for pipeline steels throughout the world (Ref 10). The microstructure of X70 and X80 pipeline steels is manipulated through TMCP, and TMCP has been shown to be an important way to control the microstructure and mechanical properties in pipeline steels (Ref 8, 11-13). The microstructure and mechanical properties of HSLA steel can be significantly improved by ultra fast cooling (UFC) after hot deformation (Ref 14, 15). UFC has been used in the plate line in recent 6 years in China, and a good deal of pipeline steels was produced using this advanced technology.

In the current study, X70 and X80 pipeline steels were fabricated by UFC processing, and their tensile and Charpy impact properties were examined. The fracture surfaces were observed in detail and the crack propagation was analyzed for Charpy impact specimens of both steels. The aim of the current article is to further investigate the role of acicular ferrite (AF) in the experimental steel subjected to UFC.

2. Experimental Procedure

The steels used in the present study were X70 and X80 grade steels, and are referred as "A" and "B", respectively. Plate thickness in rolling mill tests is 250 mm. The values of critical transformation temperatures, i.e., the start and finish of the austenite-to-ferrite transformation ($Ar3$, $Ar1$) and the nonrecrystallization temperature (Tnr) for designing the schedule of the experimental steels were experimentally obtained using a method shown in the paper (Ref 16). By using these parameters, the schedule of TMCP was designed. The chemical compositions and measured transformation temperature Tnr, $Ar3$, and $Ar1$ of the steels are listed in Table 1, and the schematic illustrations of the TMCP schedules used are shown in Fig. 1.

According to the scheme presented in Fig. 1, the plates were reheated to 1200 °C to homogenize the structure before rolling. The rough-rolling temperature started at 1150 °C above the

Yong Tian, Zhao-dong Wang, and **Guo-dong Wang**, State Key Laboratory of Rolling and Automation, Northeastern University, Shenyang 110819, China; and **Qun Li**, Department of Rolling, Qinhuangdao Shouqin Metal Materials Co, Ltd, Qinhuangdao 066326, China. Contact e-mail: tianyong@ral.neu.edu.cn.

Table 1 Chemical composition (wt.%) and measured transformation temperature (°C) of both steels

Steel	C	Si	Mn	P	S	Nb	Cr	Ni	Cu	Mo	V	Ti	B	*T*nr	*A*r3	*A*r1
A	0.087	0.168	1.610	0.011	0.006	0.075	0.021	0.011	0.021	0.002	0.003	0.012	0.0003	950	590	480
B	0.057	0.210	1.720	0.005	0.002	0.067	0.230	0.190	0.010	0.120	0.002	0.013	…	975	600	490

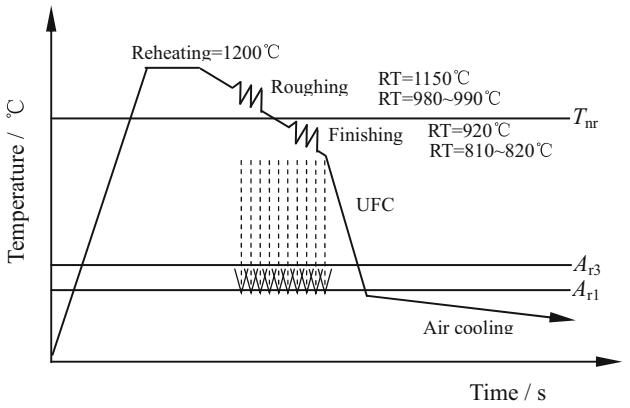

Fig. 1 Schematic illustrations describing the TMCP schedules

nonrecrystallization temperature of austenite for both steels. The finish rolling stage was started at 920 °C and finished rolling at 820 and 815 °C for steel A and B, respectively. The rolled plates steel A and B were air-cooled to the start cooling temperature of about 780 °C were water-cooled to 550 and 450 °C and then were air-cooled to room temperature. The cooling rates (water cooling) of steel A and B were 35 °C/s. The final plates with thickness of 21.4 and 22.3 mm for steel A and B, respectively, were obtained.

Ten tensile specimens, 160 mm in total length and 20 mm in effective width, 50 mm in gage length, were machined from the plates with the longitudinal axis parallel to the longitudinal direction, and tensile tests were carried out on an INSTRON 4206 machine at a strain rate of 5 mm/min at room temperature. The Charpy specimens were prepared along the rolling direction. Charpy impact tests of steels A and B were repeated five times at −10 and −15 °C, respectively, according to Chinese standard (Ref 17) to obtain an averaged result.

The morphology of the transverse section of the specimens was investigated by light optical microscopy (LOM) and scanning electron microscopy (SEM), respectively. The specimens for LOM were color etched using the LePera method (Ref 18) to reveal the ferrite, bainite, austenite and MA islands (the mixtures of brittle martensite and residual austenite), and the color etchant was a mixture of 4%$(NO_2)_3C_6H_2OH$ + saturated $Na_2S_2O_3$. With this etchant, ferrite appears gray, bainite appears black. MA islands appear white since it is difficult for them to be tinted in this etchant. The fracture appearances of Charpy specimens were visually evaluated by energy dispersive spectroscopy (EDS), in conjunction with SEM. Thin specimens were observed in a transmission electron microscopy (TEM) with energy dispersive spectrometry (EDS) facility. Volume fractions of microstructures present in the plates were measured by an image analyzer of Leica, and the area of the second phases can be automatically calculated with this image analysis software to understand the involved damage mechanisms.

3. Experimental Results

3.1 Tensile and Charpy Impact Testing Results

Ultimate tensile strength (UTS), yield strength (YS), yield ratio (YS/UTS), total elongation (TEL) of ten tensile specimens, and the Charpy absorbed energy (A_K) of five Charpy specimens including the mean and standard deviation values after UFC are summarized in Table 2.

Where M is the measured values during testing, S is the standard requirements of pipeline steels, and SD is the standard deviation values. In Table 2, UTS (633MPa), YS (553MPa), YS/UTS(0.87), and TEL (40%) were obtained for steel A, and higher UTS and YS in steel B up to 678 and 562 MPa, respectively, were achieved by UFC. Yield ratio can be reduced to less than 0.83, and TEL is not greatly reduced for steel B. It is well known that the lower the yield ratio, the better the processability for low-carbon microalloyed steels. The yield ratio of both steels is quite satisfactory.

Figure 2 shows representative stress-strain curves of both steels after UFC. These curve characteristics are almost the same as those of steel A and B. It displays a yield point upon deformation on the curves of steel A. This may be related to its relatively high ductility. On the contrary, steel B was deformed by a continuous yielding behavior.

UFC resulted in higher strength and slightly lower ductility in highly alloyed steel, and there is no clear distinction in the evaluation of impact properties between steel A and B. The Charpy absorbed energy of steel A at −10 °C was higher than 374 J, and that of steel B at −15 °C was higher than 365 J. The whole mechanical properties satisfy all the standard requirements of the X70 and X80 steels.

3.2 Optical and SEM Examination

Figure 3 reveals an overview of optical microstructure for the two LePera etched specimens after UFC.

It can be seen that the specimens consist of quasi-polygonal (QF), AF, and granular bainite (GB). The GB contains equiaxed, island-shaped martensite-austenite (MA) constituents. Large amounts of QFs coexisting with few AFs are present in steel A (Fig. 3a). Steel B specimen mostly consists of AF, together with GB. Sung (Ref 19) suggested that AF has been generalized to describe intragranularly nucleated transformation products with a relatively wide range of morphologies. Despite it is impossible to evaluate the nucleation site of the ferrite through the SEM images, AF morphologies can be easily distinguished in the SEM view.

The SEM micrographs show the presence of AFs in both steels (Fig. 4), and larger amounts of AFs are visible in steel B (Fig. 4b). Average grain size and the volume fractions of secondary phases were measured, and the results are shown in Table 3. In Table 3, Steel B has larger amounts of GB according to the measuring result of the image analysis software of Leica. Ferrite grain size was smaller in steel B. The amount of AF in steel B is much more than that in steel A.

Table 2 Mechanical properties of the experimental steels

Steels	UTS, MPa			YS, MPa			YS, UTS			TEL, %			Charpy absorbed energy, J		
	M			*M*			*M*			*M*			*M*		
	Mean	SD	*S*	Mean	SD	*S*	Mean	SD	*S*	Mean	SD	*S*	Mean	SD	*S*
Steel A (X70)	633	27.10	570 to 760	553	30.48	500 to 635	0.87	0.03	0.9	40	2.79	24	374 (−10 °C)	58.15	85
Steel B (X80)	678	15.50	625 to 825	562	23.59	530 to 670	0.83	0.03	0.9	35	3.34	24	365 (−15 °C)	64.11	200

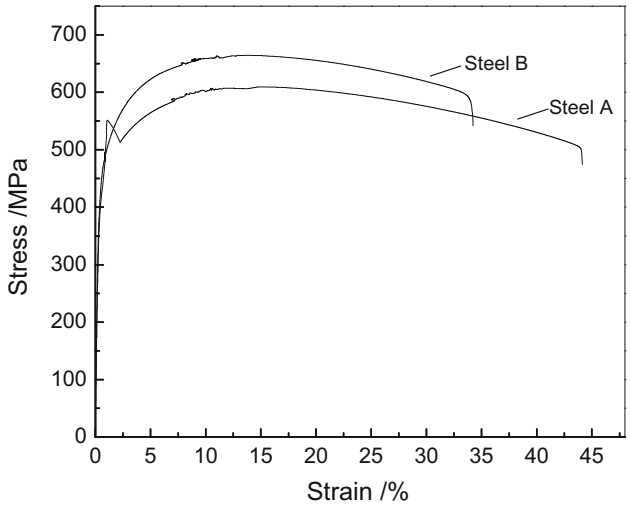

Fig. 2 Stress-strain curves of both steels (a) steel A; (b) steel B

Moreover, finely dispersed MA islands were observed, and the volume fraction of MA in steel B is higher than that in steel A. The differentiation of the volumetric fraction of the MA constituent was revealed through LePera etch (as described above). There are a lot of white color secondary phases which may be cementite, retained austenite, and martensite-austenite constituents in the specimen etched with 4% natal for steel B.

3.3 Fractographic Analysis

The fractographic views of the Charpy specimens of both steels after UFC are shown in Fig. 5. Shear lips are visible, surrounding fibrous and radial region. Both steels are all characterized with a ductile fracture feature. Fibrous regions in steel B are somewhat smaller than those in steel A. Large dimples are formed at locations of the fibrous regions for both steels, as seen in Fig. 6 and 7. Microvoids form at inclusions and energy dispersive spectrometry (EDS) microanalysis results show that these inclusions are nonmetallic constituents or other compounds. The mixed fracture mechanism which consists of cleavage fracture surfaces and dimples exist together in the radial region. This type of fracture is called quasi-cleavage fracture surface (Ref 20) (Fig. 8).

3.4 TEM Analysis

TEM bright-field image, Fig. 9(a), shows a representative area of the general microstructure of QF and AF in steel A. The final microstructure after UFC exhibits a representative characteristic of a needlelike appearance and a relatively high dislocation density in steel B (Fig. 9b). Moreover, TEM studies also confirm the presence of the MA constituent among the subgrains (Fig. 10), and MA island is fine and dispersed in steel B (Fig. 10b). In Fig. 11, 12, the TEM view displays very fine precipitates. The precipitation should take place in austenite during hot rolling according to the distribution and sizes of precipitates showed in the micrographs. These nanoprecipitates are carbides and carbonitrides which are likely to form at lower temperatures during or after UFC.

4. Discussion

Analytical strengthening mechanism are necessary to understand the effects of UFC processing on microstructure and mechanical properties of pipeline steels. The alloying elements in the experimental steels increase the hardenability of austenite and leads to solid solution strengthening. The fine Nb/Ti (C, N) particles not only provided precipitation strengthening, but refined the ferrite grains because they restricted austenite grain growth (Ref 21). Higher strength levels are attributed to the strengthening contribution caused by precipitation strengthening and grain refinement. Steel B has higher UTS and YS because it has larger amounts of GB due to higher Mo content. The addition of Ni lowers the ductile-brittle transition temperature, and thus the Charpy absorbed energy of steel B was satisfactory.

UFC directly results in the improvement of mechanical properties. The size and distribution of precipitates (Nb/Ti carbonitrides) in steel B are finer and more dispersed than those in steel A due to relatively low finish cooling temperature. This is one important reason that the mechanical properties of steel B were higher than those of steel A. It was noted that a visible high dislocation density existed in the specimen of steel B (Fig. 9b), which can increase the strength of this steel. Nevertheless, the role of the strengthening contribution caused by grain refinement could not be ignored.

The rolling at γ nonrecrystallization region accumulates a strain (i.e., dislocations) in austenite grains and this strain can promote the ferrite grain refinement by acting as a nucleation site for γ-α transformation (Ref 22). The grain size is generally affected by the cooling rate (Ref 23). The ferrite grain size of both steels can be further refined by an UFC rate. It is well known that grain refinement is the strengthening mechanism that simultaneously improves both strength and toughness. Consequently, UFC processing improves not only UTS, YS, YS/UTS, and TEL of both steels, but their Charpy absorbed energy as well.

Note that the Charpy absorbed energies of steel B do not significantly reduce despite test was performed at relatively low temperature (Table 2). It relates to the microconstituents of the steel after UFC. MA islands are more finely dispersed in steel B

(Table 3). These finely dispersed MA islands not only provide dispersion strengthening, but also reduce loss of impact properties to pipeline steels. A small size distribution of MA islands impedes dislocation motion in a ferrite matrix. The tendency for cracking decreases as the stress concentrations reduce. Therefore, higher strength and toughness are also attributed to the presence of substantially finely dispersed MA islands and precipitates, despite a certain extent loses toughness.

UFC produces low-temperature transformation microstructures containing a significant amount of AFs. A substantial amount of AFs plays a key role for the experimental steels. The AF nucleates at intragranular sites and it is characterized by an assemblage of interwoven nonparallel ferrite laths with high density of tangled dislocations, where the most part of the neighboring lath (subgrain) boundaries have dissimilar orientations (Ref 24). Nonmetallic inclusions can act as nucleation sites for AF (Ref 25). Steel B may contain larger amounts of AF because it was cooled rapidly to a relatively low finish cooling temperature. Schematic illustrations of the crack propagation path in both steel specimens are shown in Fig 13(a) and (b), respectively, without regard to the presence of MA islands.

In Fig. 13(b), there are more twists and turns of a crack growth curve in steel B in which AF is the major phase. As mentioned above, the amount of AF in steel B is much more than that in steel A. There are significant barriers to a growing cleavage crack in steel B because of a great deal of AF grain boundary. Therefore, it is more difficult for crack propagation in steel B. A microstructure of AF has the potential of combining high strength and high toughness, because a crack would have to follow a more tortuous path through a microstructure of AF (Ref 26). Thus, the toughness of steel B

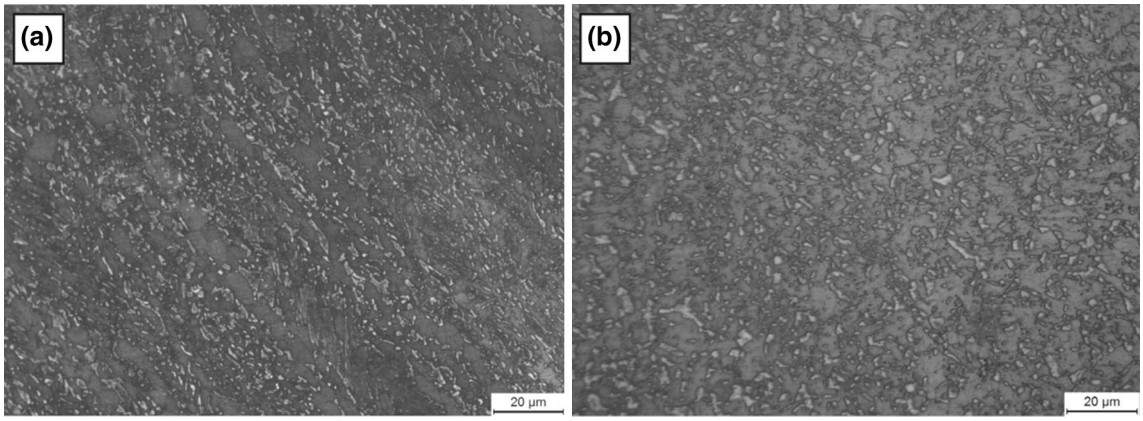

Fig. 3 Optical micrographs of both steels after UFC (by LePera etched) (a) steel A; (b) steel B

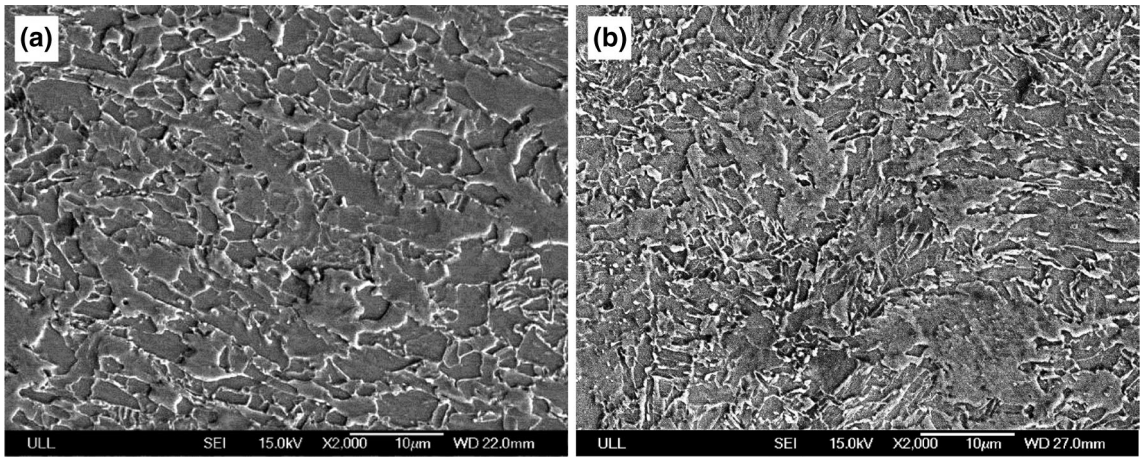

Fig. 4 SEM micrographs of both steels after TMCP (a) steel A; (b) steel B

Table 3 Average grain size and the size and the volume fractions of secondary phases

Steel	Quasi-polygonal ferrite	Acicular ferrite	Granular bainite, %	Average grain size, μm	The volume fractions of secondary phases, %	The size of secondary, μm phases, μm	Average size of secondary, μm phases, μm
A	Bal.	…	12	9.91	18.85	3.25 to 4.77	4.01
B	…	Bal.	19	8.56	23.81	2.63 to 4.21	3.42

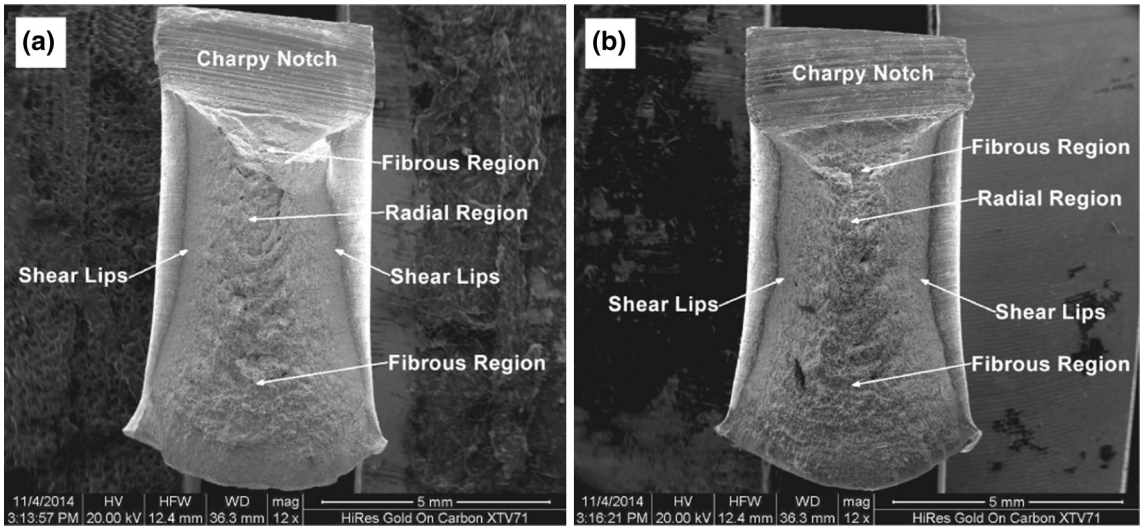

Fig. 5 The macroscopic appearances of fracture surfaces of both steels (a) the fibrous regions; (b) EDS pattern for inclusion particle

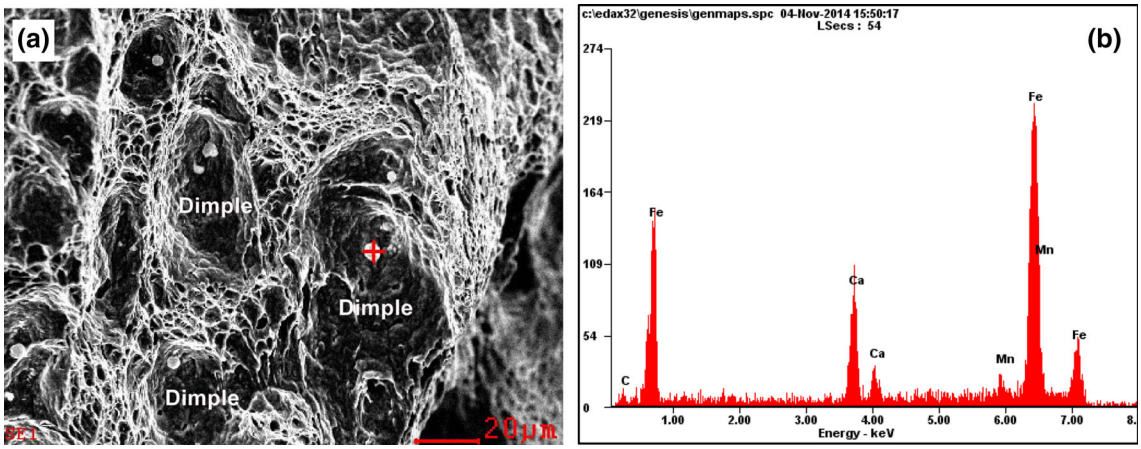

Fig. 6 The microscopic appearance of fracture surfaces of steel A (a) the fibrous regions; (b) EDS pattern for inclusion particle

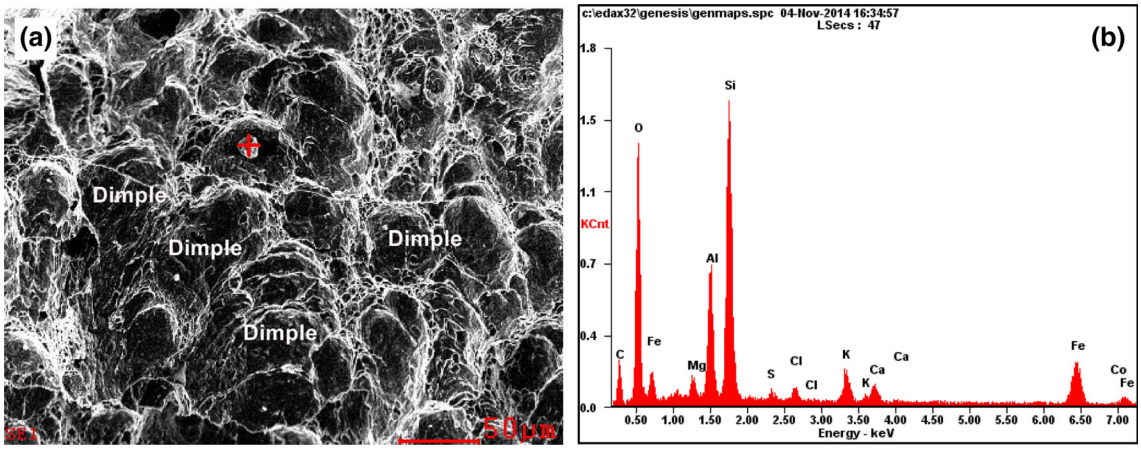

Fig. 7 The microscopic appearance of fracture surfaces of steel B (a) steel A; (b) steel B

is no worse than that of the steel A considerably. The presence of larger amounts of AF is the primary reason, that is, the toughness of the experimental steel increases with increasing the amount of AF. As a result, fractographic evidence of the Charpy specimens exhibits characteristics of ductile for both steels after UFC (Fig. 5 to 8).

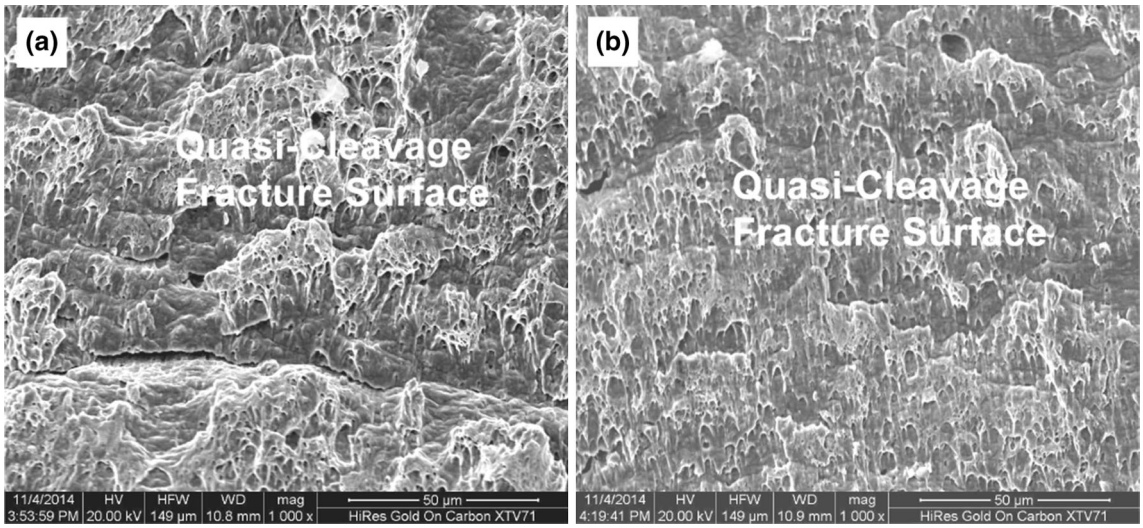

Fig. 8 Quasi-cleavage fracture surfaces of both steels (a) steel A; (b) steel B

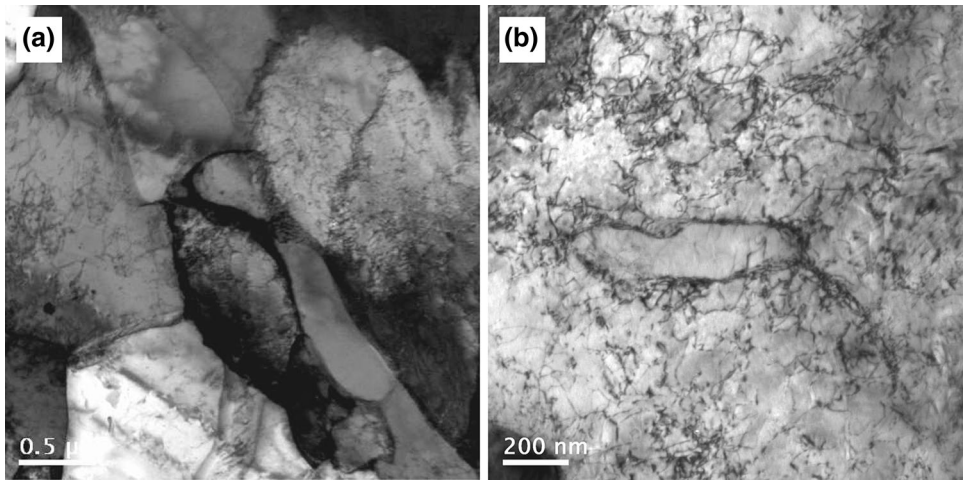

Fig. 9 QF and AF in both steels (a) steel A; (b) steel B

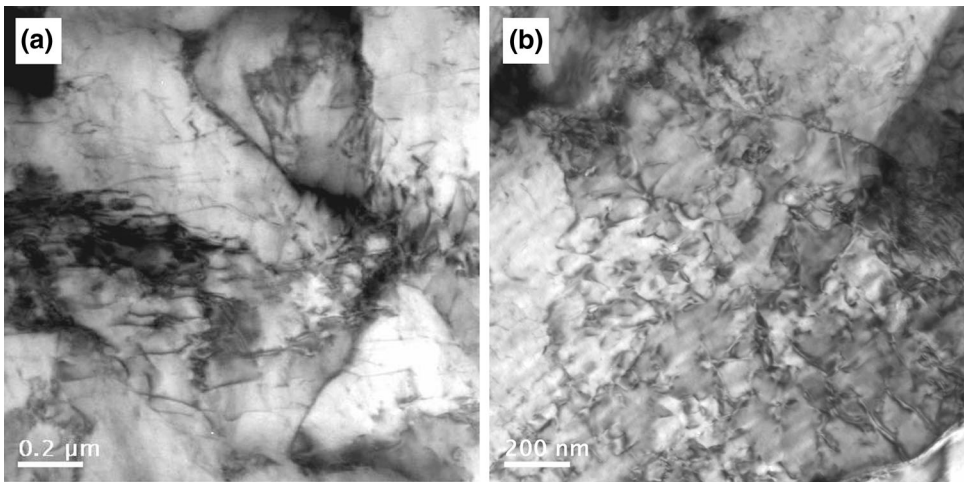

Fig. 10 MA islands in both steels (a) the precipitate particles; (b) EDS image

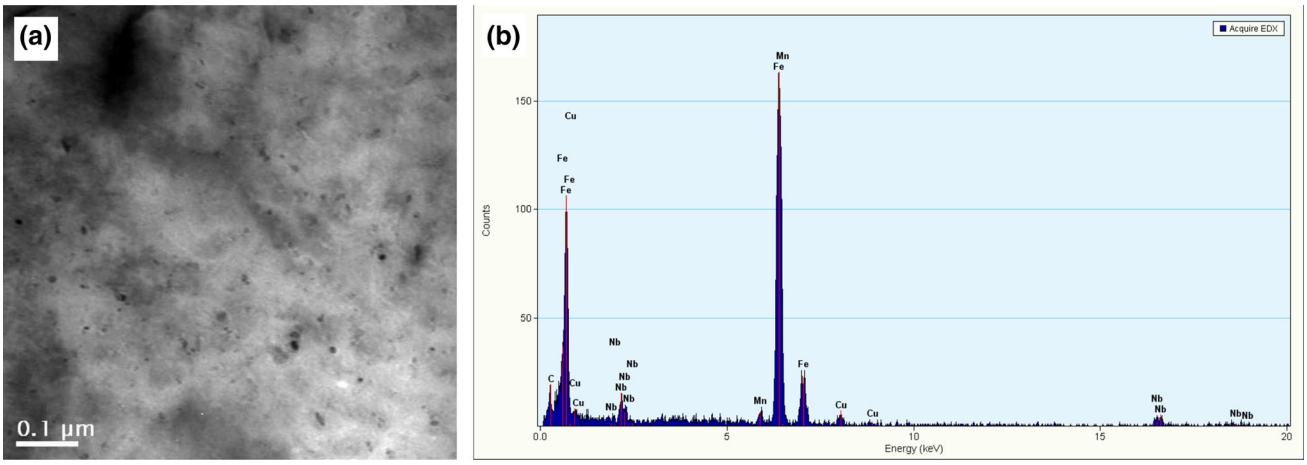

Fig. 11 TEM micrograph of steel A (a) the precipitate particles; (b) EDS image

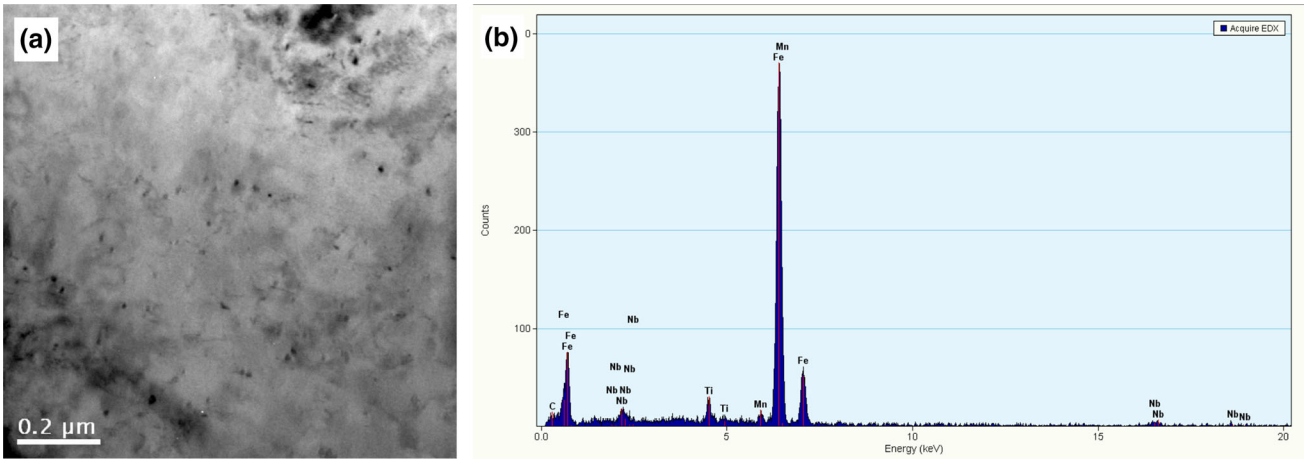

Fig. 12 TEM micrograph of steel A (a) steel A; (b) steel B

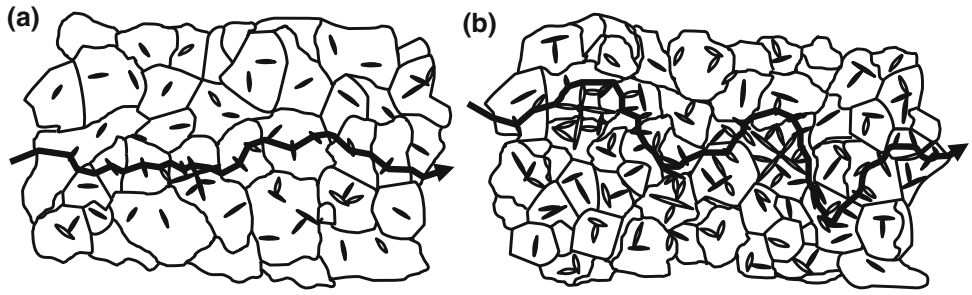

Fig. 13 Schematic illustrations of crack propagation path in both steels

5. Conclusions

The following conclusions can be drawn from this study.

1. X70 and X80 pipeline steels were fabricated by UFC processing. The microstructures of both steels were all composed of QF, AF, and GB. MA islands are more finely dispersed in steel B, and the amount of AF in steel B is much more than that in steel A because of UFC processing.
2. UFC resulted in higher mechanical properties for both steels. This is mainly attributed to the effect of the grain refinement, except for the strengthening contribution caused by solid solution and precipitation strengthening, because UFC significantly refined the ferrite grain size. The size and distribution of precipitates (Nb/Ti carboni-

trides) in steel B are finer and more dispersed than those in steel A due to relatively low finish cooling temperature. Consequently, the strength of steel B was higher than that of steel A.

3. Quasi-cleavage fracture surfaces were observed in both steels. Fractographic evidence of the Charpy specimens after UFC exhibits characteristics of ductile. A small size distribution of MA islands impedes dislocation motion in a ferrite matrix. The tendency for cracking decreases as the stress concentrations reduce. Therefore, the finely dispersed MA islands not only provide dispersion strengthening, but also reduce loss of impact properties to pipeline steels.
4. UFC produces low-temperature transformation microstructures containing larger amounts of AFs. The presence of AF is a crucial factor in achieving desired mechanical properties for both steels. There are more twists and turns of a crack growth curve in steel B in which AF is the major phase. Therefore, it is more difficult for crack propagation in steel B. It is suggested that the toughness of the experimental steel increases with increasing the amount of AF.

Acknowledgment

This work was supported by the Natural Science Foundation of China (Grant No. 51234002). The authors are grateful to the staff of Qinhuangdao Shouqin Metal Materials Co, Ltd.

References

1. V.V. Orlov, V.A. Malyshevskii, E.I. Khlusova, and S.A. Golosienko, Production Technology for Arctic Pipeline and Marine Steel, *Steel Trans.*, 2015, **44**, p 696–705
2. Z.X. Zhu, L. Kuzmikova, H.J. Li, and F. Barbaro, The Effect of Chemical Composition on Microstructure and Properties of Intercritically Reheated Coarse-Grained Heat-Affected Zone in X70 Steels, *Metall. Mater. Trans. B*, 2014, **45**, p 229–235
3. L.K. Ji, H.L. Li, H.T. Wang, J.M. Zhang, W.Z. Zhao, H.Y. Chen, Y. Li, and Q. Chi, Influence of Dual-Phase Microstructures on the Properties of High Strength Grade Line Pipes, *J. Mater. Eng. Perform.*, 2014, **23**, p 3867–3874
4. M. Zhu, C.W. Du, X.G. Li, Z.Y. Liu, S.R. Wand, T.L. Zhao, and J.H. Jia, Effect of Strength and Microstructure on Stress Corrosion Cracking Behavior and Mechanism of X80 Pipeline Steel in High pH Carbonate/Bicarbonate Solution, *J. Mater. Eng. Perform.*, 2014, **23**, p 1358–1365
5. M. Allouti, C. Schmitt, and G. Pluvinage, Assessment of a Gouge and Dent Defect in a Pipeline by a Combined Criterion, *Eng. Fail. Anal.*, 2014, **36**, p 1–13
6. R. Shukla, S.K. Das, K.B. Ravi, S.K. Ghosh, S. Kundu, and S. Chatterjee, An Ultra-low Carbon, Thermomechanically Controlled Processed Microalloyed Steel: Microstructure and Mechanical Properties, *Metall. Mater. Trans. A*, 2012, **43**, p 4835–4845
7. N. Isasti, D.J. Badiola, M. Taheri, and P. Uranga, Phase Transformation Study in Nb-Mo Microalloyed Steels Using Dilatometry and EBSD Quantification, *Metall. Mater. Trans. A*, 2013, **44A**, p 3552–3563
8. P.S. Bandyopadhyay, S.K. Ghosh, S. Kundu, and S. Chatterjee, Evolution of Microstructure and Mechanical Properties of Thermomechanically Processed Ultrahigh-Strength Steel, *Metall. Mater. Trans. A*, 2011, **42A**, p 2742–2752
9. H. Aydin and T.W. Nelson, Microstructure and Mechanical Properties of Hard Zone in Friction Stir Welded X80 Pipeline Steel Relative to Different Heat Input, *Mater. Sci. Eng. A*, 2013, **586**, p 313–322
10. S. Nafisi, M.A. Arafin, L. Collins, and J. Szpunar, Texture and Mechanical Properties of API, X100 Steel Manufactured under Various Thermomechanical Cycles, *Mater. Sci. Eng. A*, 2012, **531**, p 2–11
11. V.C. Olalla, V. Bliznuk, N. Sanchez, P. Thibaux, L.A.I. Kestens, and R.H. Petrov, Analysis of the Strengthening Mechanisms in Pipeline Steels as a Function of the Hot Rolling Parameters, *Mater. Sci. Eng. A*, 2014, **604**, p 46–56
12. M. Opiela, Effect of Thermomechanical Processing on the Microstructure and Mechanical Properties of Nb-Ti-V Microalloyed Steel, *J. Mater. Eng. Perform.*, 2014, **23**, p 3379–3388
13. X.J. Liang and A.J. Deardo, A Study of the Influence of Thermomechanical Controlled Processing on the Microstructure of Bainite in High Strength Plate Steel, *Metall. Mater. Trans. A*, 2014, **45A**, p 5173–5184
14. S.V. Ravikumar, J.M. Jha, S.S. Mohapatra, S.K. Pal, and S. Chakraborty, Influence of Ultrafast Cooling on Microstructure and Mechanical Properties of Steel, *Steel Res. Int.*, 2013, **84**, p 1157–1170
15. X.W. Kong, L.Y. Lan, Z.Y. Hu, B. Li, and T.Z. Sui, Optimization of Mechanical Properties of High Strength Bainitic Steel Using Thermomechanical Control and Accelerated Cooling Process, *J. Mater. Process. Technol.*, 2015, **217**, p 202–210
16. Z. Li and D. Wu, Effects of Hot Deformation and Subsequent Austempering on Mechanical Properties of High Silicon and Low Silicon TRIP steel, *Mater. Sci. Technol.*, 2008, **24**, p 168–176
17. National Standard of the People's Republic of China. Petroleum and Natural Gas Industries-Steel Pipe for Pipeline Transportation Systems. GB/T 9711-2011, Beijing: Chinese Standard Press, 2011, p 27
18. E. Girault, P. Jacques, P. Harlet, K. Mols, J.V. Humbeek, E. Aernoudt, and F. Delannay, Metallographic Methods for Revealing the Multiphase Microstructure of TRIP-Assisted Steels, *Mater. Charact.*, 1998, **40**, p 111–118
19. H.K. Sung, S.Y. Shin, B. Hwang, C.G. Lee, and S. Lee, Effects of Cooling Conditions on Microstructure, Tensile Properties, and Charpy Impact Toughness of Low-Carbon High-strength Bainitic Steels, *Metall. Mater. Trans. A*, 2013, **44**, p 294–302
20. M.J. Kang, H. Kim, S. Lee, and S.Y. Shin, Effects of Dynamic Strain Hardening Exponent on Abnormal Cleavage Fracture Occurring During Drop Weight Tear Test of API, X70 and X80 Linepipe Steels, *Metall. Mater. Trans. A*, 2014, **45**, p 682–697
21. J. Kim, J.G. Jung, D.H. Kim, and Y.K. Lee, The Kinetics of Nb(C, N) Precipitation During the Isothermal Austenite to Ferrite Transformation in a Low-Carbon Nb-Microalloyed Steel, *Acta Mater.*, 2013, **61**, p 7437–7443
22. Y.W. Kim, S.W. Song, S.J. Seo, S.G. Hong, and C.S. Lee, Development of Ti and Mo Micro-alloyed Hot-Rolled High Strength Sheet Steel by Controlling Thermomechanical Controlled Processing Schedule, *Mater. Sci. Eng. A*, 2013, **565**, p 430–438
23. M. Grny and G. Sikora, Effect of Titanium Addition and Cooling Rate on Primary α(Al) Grains and Tensile Properties of Al-Cu Alloy, *J. Mater. Eng. Perform.*, 2015, **24**, p 1150–1156
24. E.V. Morales, R.A. Silva, I.S. Bott, and S. Paciornik, Strengthening Mechanisms in a Pipeline Microalloyed Steel with a Complex Microstructure, *Mater. Sci. Eng. A*, 2013, **585**, p 253–260
25. C. Capdevila, C.G. Mateo, J. Chao, and F.G. Caballero, Effect of V and N Precipitation on Acicular Ferrite Formation in Sulfur-Lean Vanadium Steels, *Metall. Mater. Trans. A*, 2009, **40A**, p 522–538
26. I.R.V. Pedrosa, C.R.S. De, Y.P. Yadava, and R.A.S. Ferreira, Study of Phase Transformations in API, 5L X80 Steel in Order to Increase its Fracture Toughness, *Mater. Res.*, 2013, **16**, p 489–496